Journal of Materials Chemistry C

ROYAL SOCIETY OF CHEMISTRY

PAPER

View Article Online
View Journal | View Issue

Cite this: J. Mater. Chem. C, 2026, 14, 1244

Improving SERS sensitivity *via* hot spots and control of molecular orientation

Guru P. Neupane * and Rahul K. Salaria

Surface-enhanced Raman spectroscopy (SERS) is a high-throughput, surface-sensitive and label-free analytical technique that provides the molecular fingerprints of bio/chemical analytes. The quality of SERS signals of analytes mainly relies on the electromagnetic field strength generated by nanostructured platforms. In this regard, this article describes a new strategy for enhancing SERS intensity by the integration of hotspot engineering and parallel orientation of molecules to a nanostructure (NS) surface. We investigate the relationship between the nanostructure geometry and the molecular orientation to enhance the SERS intensity of a few thiol-derivative reporter molecules including 4-mercaptophenol (4-MCP), 4-mercaptobenzoic acid (4-MBA), and 4-mercaptophenyl boronic acid (4-MPBA), using Au nanoflowers (NFs) and nanorods (NRs). This study demonstrates a significant enhancement in the relative SERS intensity of aromatic ring breathing vibrations as well as many other skeleton-based bond vibrations of the reporter molecules, observed from Au NF arrays. This study offers a strategic opportunity for the future development of highly efficient bio/chemical sensors, such as pH sensors, glucose sensors, *etc.*, that require monitoring of selective vibrational bonds in those reporter molecules. This study can be an important experimental illustration for an elaborate understanding of the SERS phenomena as well as for the future development of biosensing technologies.

Received 21st July 2025,
Accepted 5th November 2025

DOI: 10.1039/d5tc02771c

rsc.li/materials-c

Introduction

Surface-enhanced Raman spectroscopy (SERS) is a high-throughput and label-free analytical technique used in both basic and applied scientific research. The SERS technique has been utilized to identify molecular bond vibrations and atomic lattice vibrations with remarkably higher sensitivity.[1,2] The capability of this technique to enhance the Raman intensity by up to 10^8 relative to normal Raman,[2,3] along with its ability to rapidly detect a tiny number of bio/chemical analytes even down to a single molecule in special cases,[4,5] has increased its importance to develop ultra-sensitive chemical and biomolecular sensors useful for environmental and medical applications.[6–11] However, there are still some ambiguities in explaining the SERS phenomenon, particularly regarding various possible factors that can influence the resulting SERS spectra. In this context, this article aims to advance the understanding of SERS phenomena to design more efficient SERS based bio/chemical nano sensors.

Many studies have shown that the localization of bio/chemical molecules to metallic nanostructures (NSs) and their morphology can hugely manipulate the SERS sensitivity.[6,8,12] Specifically, hotspot engineering of NSs, such as crevices, edges, spikes, petals, *etc.*, is a key process for the improvement of SERS sensitivity.[13–15] Recently, a few studies have further emphasized that SERS sensitivity also relies on the orientation of molecules relative to the surface of metallic NSs.[16–18] Scher *et al.* highlighted that the nature of sulfur hybridization of a thiol derivative reporter molecule onto a NS surface determines the sulfur–carbon (S–C) bond angle to the NS surface, which in turn influences the molecular orientation on the NSs.[16] For example, sp^3 hybridization of sulfur on a gold (Au) surface leads to a 104° bond angle (nearly parallel orientation) at very low concentrations of molecules. However, in the presence of high-density molecules crowding the Au surface, the steric force of repulsion can turn a parallel orientation to perpendicular to the Au surface. On the other hand, the sp hybridization of sulfur onto a silver (Ag) surface leads to a ~180° bond angle (nearly perpendicular), despite the concentration of reporter molecules.

Herein, we study the SERS activity of Au nanoflowers (NFs) and nanorods (NRs) functionalized with a few SERS-active thiol derivative reporter molecules to investigate the relationships among NSs' geometry, molecular orientation, and SERS intensity. Our study illustrates that the unique geometry of Au NFs can provide a great opportunity for the integration of hotspots and parallel orientations of functionalized molecules on the surface of the NSs. Such a unique integration significantly improves the relative SERS sensitivity of aromatic ring

Department of Biomedical Engineering, Northwestern University, Evanston, IL-60208, USA. E-mail: guru.neupane@northwestern.edu

breathing vibrations as well as many other skeletal bond vibrations. We validate the findings with three thiol derivative aromatic molecules, including 4-mercaptophenol (4-MCP), 4-mercaptobenzoic acid (4-MBA), and 4-mercaptophenyl boronic acid (4-MPBA). A significant improvement in the relative SERS intensity of such bond vibrations can be useful for the development of highly efficient pH and glucose sensing applications.[7,19–21] On the other hand, these selected functional molecules can form a coordination complex with Au NSs,[22,23] which can also be an effective plasmonic probe for monitoring various bio-enzymes. We believe that this study can be important to advance the understanding of SERS phenomena as well as to develop efficient bio/chemical sensors.

Results and discussion

Synthesis and characterization of Au NSs

There are many techniques to synthesize various types of NSs, such as chemical, hydrothermal, solvothermal, chemical vapor deposition, exfoliation methods, *etc.*[24–30] In this work, we synthesized Au NFs and Au NRs based on the chemical solution method. We used surfactant-free and seedless aqueous solutions to synthesize Au NFs.[31] Injecting 0.64 mL of hydroxylamine hydrochloride (0.1 M), 1 mL of sodium citrate dibasic (0.1 M), 0.8 mL of sodium hydroxide (0.1 M) solutions and 1 mL of tetrachloroauric(III) acid (0.01 M) into 20 mL of water under vigorous stirring resulted in the formation of beautiful Au NFs. Fig. 1(a) shows scanning electron microscopy (SEM) images of Au NFs. The average lateral size (diameter) of Au NFs was found to be ~80 nm. During the synthesis of Au NFs, each solvent plays a unique role, that is, hydroxylamine acts as a reductant, trisodium citrate as a stabilizer, sodium hydroxide as a pH regulator, and tetrachloroauric(III) acid as a gold precursor. This synthesis process is a one-step nucleation process, and the vigorous stirring of the mixture promotes very fast and anisotropic growth, which results in shaping the NSs to flower-like structures. Indeed, hydroxylamine typically reduces the tetrachloroauric(III) acid into a gold seed in aqueous solution and promotes the anisotropic growth of flower-like structures.[32,33] Fast reaction kinetics play a crucial role in this growth process, and the high pH value of the growth solution predominantly controls these kinetics. Therefore, prior to the addition of the gold precursor, a suitable pH of the solution should be achieved by controlling the concentrations and volume ratio of hydroxylamine and sodium hydroxide, as previously reported. We mixed a tiny amount of polyvinylpyrrolidone (PVP) (resulting concentration: 50 nM) with the Au NF colloidal solution to keep these Au NFs stable for many days.

We followed a silver assisted seed mediated method to grow Au NRs.[7,34] An Au seed solution was prepared by mixing aqueous solutions of 0.25 mL of tetrachloroauric(III) acid (0.01 M), 9.75 mL of cetyltrimethylammonium bromide (CTAB) (0.1 M), and 600 μL of ice-cold sodium borohydride (0.01 M) under vigorous stirring. Furthermore, the growth solution was separately prepared by mixing aqueous solutions of 9.11 mL of CTAB (0.1 M), 0.13 mL of silver nitrate (0.01 M), 0.5 mL of tetrachloroauric(III) acid (0.01 M), 0.19 mL of HCl (1 M), and 0.08 mL of ascorbic acid (0.1 M). After an hour of seed aging, 24 μL of the seed solution was mixed to the growth solution and kept overnight to grow Au NRs. Then, the Au NR colloidal solution was centrifuged twice at 10 000 rcf for 30 min and the supernatant was removed. Finally, the sediment of Au NR pellets was dispersed in the same volume of Milli-Q H_2O and stored at 4 °C in a refrigerator for future use. These Au NRs are chemically and physically stable for a few months. Fig. 1(b) shows SEM images of Au NRs; the average size of Au NRs was found to be ~15 nm × 55 nm.

Fig. 1(c) shows the corresponding ultraviolet-visible (UV-vis) light extinction spectra of Au NFs and NRs, which were used for our SERS study. Au NRs exhibit two plasmonic extinction peaks at ~550 nm and ~770 nm (black line), which are respectively referred to as the transverse and longitudinal plasmonic modes of Au NRs. Similarly, Au NFs exhibit a broad plasmonic extinction spectrum with a peak at ~770 nm (red line). Such a broad peak could arise due to a large surface area and anisotropic flower-like structures.[35,36] The formation of Au NFs and NRs is also clearly visualized with the colors of colloidal solutions, as shown in the inset images of Fig. 1(c).

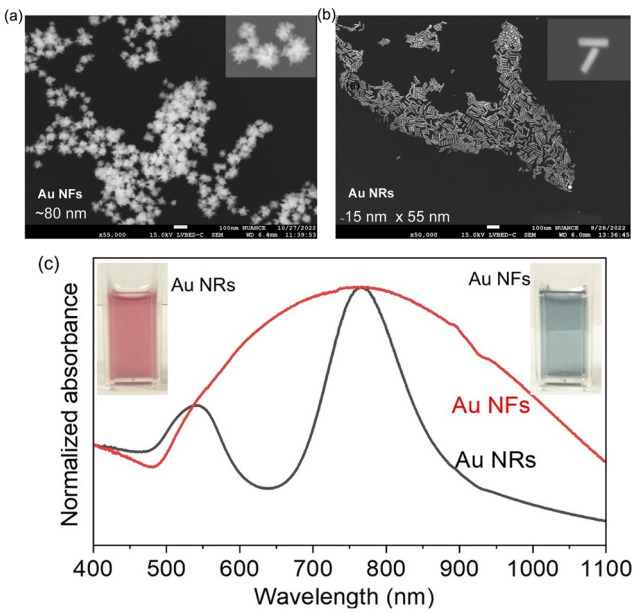

Fig. 1 Characterization of Au NSs. SEM images of (a) Au NRs and (b) Au NFs (scale bar, 100 μM). The inset images show zoomed images of Au NRs and NFs. (c) UV-vis extinction spectra of Au NR (black curve) and Au NF (red curve) colloidal solutions. The inset images show camera images of the colloidal solutions of Au NRs and NFs.

SERS activity of Au NRs and Au NFs

We prepared the sample on silicon (Si) chips for the SERS measurement. Overnight incubation of oxygen plasma-treated Si-chips in a solution containing 40 μL of Au NS colloidal solution, along with 960 μL of a 1 : 1 ethanol–water solution, resulted in good adsorption of Au NSs onto Si-chips. Indeed, oxygen plasma treatment bombards the silicon surface with

reactive oxygen species and forms Si–O or Si–OH bonds. These oxygen-rich sites can easily interact with Au atoms *via* orbital overlap, resulting in covalent or semi-covalent bonding linkages, Si–O–Au. These linkages are stronger than physisorption and effectively anchor gold atoms or clusters to the silicon surface. The Si–O–Au interaction lowers the overall interfacial energy, making adsorption more spontaneous and thermodynamically favorable.[37,38] After rinsing the Si-chips containing Au NSs with water and ethanol and air drying, we incubated them again in a 1 mM solution of the reported functional molecules for about 5 hours. Then, after rinsing them with water and ethanol and air drying, the SERS measurement was carried out. These reporter molecules are bonded to the Au surface *via* thiol-bonding, which involves the interaction between the thiol groups (–SH) of reporter molecules and Au NSs. Such –SH binding provides the availability of numerous molecular bond vibrations at around 1 nm distance from the surface of Au NSs.[11]

The surface chemistry of the NSs, NS-reporter molecules' mode of interaction and the concentration of reporter molecules significantly impact the SERS signal.[39–41] Au NRs provide two distinct plasmonic modes: transverse and longitudinal modes at ~550 nm and ~770 nm, respectively, which allow the surface plasmon resonance (SPR) effects. The unique flower-like structures of Au NFs provide such an SPR effect at 770 nm. We conducted the SERS measurement using a 788 nm laser with an exposure time of 10 s. To determine a suitable laser power that avoids potential laser power-induced heating effects in the SERS spectra, we first carried out laser power-dependent SERS measurements of 4-MPBA molecules adsorbed on Au NRs. As shown in SI Fig. S1, the SERS peaks remained consistent at excitation power below 3.49 mW, confirming a thermally safe range. Accordingly, we chose a laser power of 2 mW for all subsequent SERS experiments, which is much below the threshold (~3.5 mW) and still yields a strong SERS signal from the reporter molecules.

Fig. 2 shows the surprising increase in the Au NF assisted relative SERS peak intensity of aromatic ring breathing vibration (~1588 cm^{-1}) of all the chosen reporter molecules, 4-MBA, 4-MPBA and 4-MCP at 1 mM concentrations, with respect to C–S stretching vibration (~1080 cm^{-1}), in comparison with Au NRs. We observed that the Au NF assisted SERS intensity enhancement factors are 6.8 times higher for 4-MCP, 3.1 times higher for 4-MPBA and 2.7 times higher for 4-MBA molecules compared to the Au NR assisted signals. We believe that possible changes in the orientation of reporter molecules to the Au NFs and the numerous hot spots available in their petal-like structures could be responsible for increasing the relative SERS intensity of the aromatic ring breathing modes of these molecules. The molecular orientation to the surface of NSs

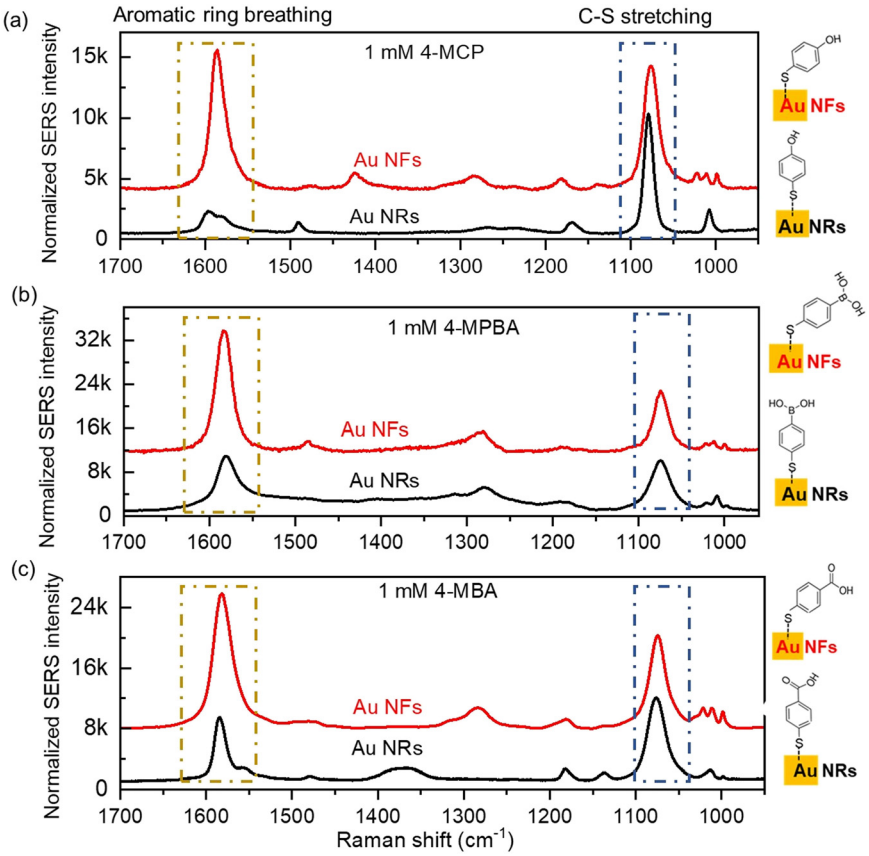

Fig. 2 Comparison of SERS sensitivity between Au NRs and NFs. SERS signals of 1 mM concentration of various molecules: (a) 4-MCP, (b) 4-MPBA, and (c) 4-MBA. Schematic images illustrate the proposed molecular orientation.

usually doesn't impact the C–S bond vibration, as it always remains closer to the NS surface. However, other ring breathing modes can be hugely affected by changes in the molecular orientation, which causes the changes in their proximity to the NS surface. Recent studies have shown that molecular orientations particularly rely on the concentration of reporter molecules and NS material types.[16,17] With regard to the material types, the sp3 hybridization for sulfur on the Au surface and sp hybridization for sulfur on the Ag surface lead to different preferred bond angles, ~104° for Au–S–C *vs.* ~180° for Ag–S–C, respectively.[42,43] Hence, more parallel molecular orientation with respect to the Au surface and perpendicular molecular orientation with respect to the Ag surface can be expected. However, regardless of sulfur hybridization, molecular concentration has also been found responsible for altering their orientation on the Au flat surface.[16] At higher concentrations, molecules could reorient from parallel to perpendicular on the Au surface possibly due to the steric repulsion of molecules at their high density crowd on Au NSs.[44] In our case, the large surface area of Au NFs and their petals with irregular anisotropic geometry may cause a more parallel orientation of reporter molecules compared to Au NRs, despite both Au NSs being functionalized with the same 1 mM concentration of each reporter molecule.

Early studies have shown that the roughness of NSs can significantly alter the orientation of the adsorbed molecules onto the NSs' surface.[45–48] For example, the convex surfaces induce different strain and steric constraints and that can alter the binding angles and orientations.[48] Moreover, Villarreal *et al.* pointed out the mechanism of binding and orientations of thiol groups (–SH) to the Au surface.[49] They concluded that the convex surfaces may promote radial molecular orientations with reduced lateral interactions, while the molecules on the concave surface may experience alterations in their tilt angles. DFT calculations have also revealed that adsorption geometries are not just energetically favorable but also geometrically constrained.[50] Considering such progress, we trust that the large area and a unique hierarchical structure of Au NFs could possibly favor the molecular orientation to be more parallel to the Au NF petals even at high density molecular clouds. This condition can support the closer proximity of molecules to the Au NF surface. Hence the presence of numerous hot spots and the close proximity of functional reporter molecules to Au NFs could be responsible for the higher relative SERS intensity of the aromatic breathing vibration mode observed with Au NFs compared to Au NRs.

Fig. 3 shows the comparisons of the SERS peak positions associated with the aromatic ring breathing mode and C–S vibrational modes of these three reporter molecules generated by Au NFs and NRs. We observed the significant shifts in the SERS peak position of the aromatic breathing mode generated by Au NFs relative to Au NRs. The SERS peak position shifts in

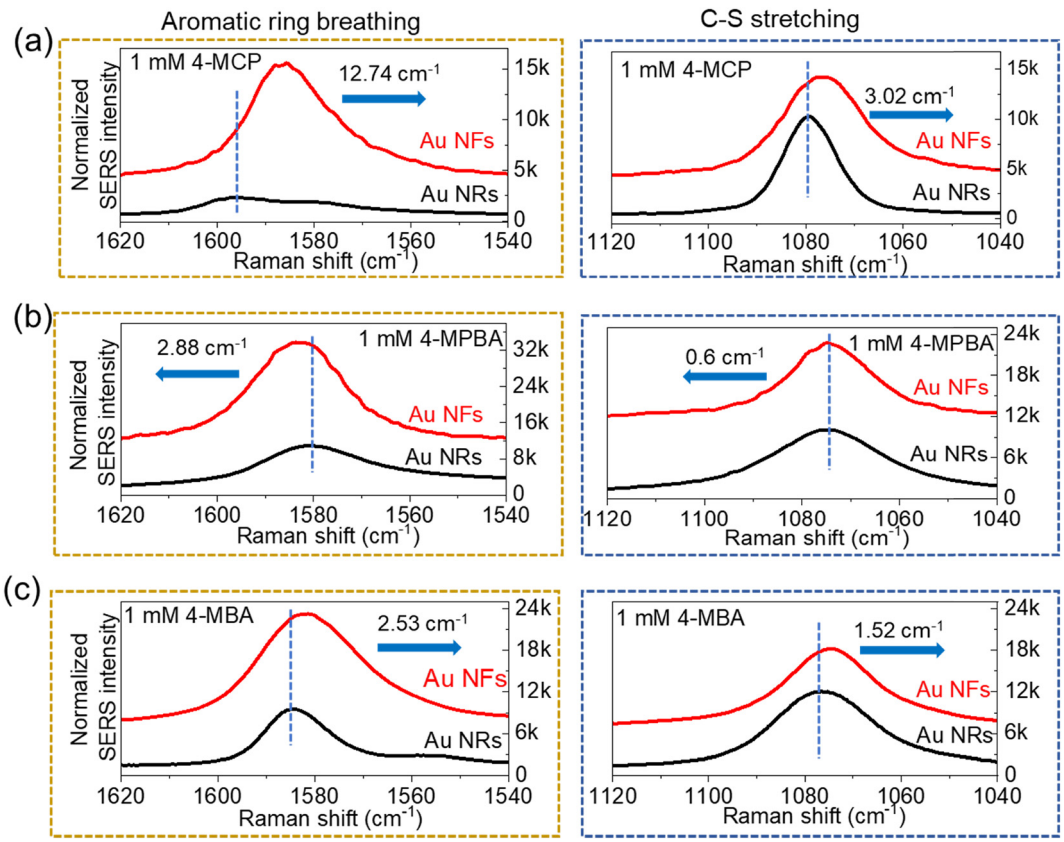

Fig. 3 Comparison of peak positions of SERS signal assigned to aromatic ring breathing modes and C–S stretching bond vibration at 1 mM concentration of (a) 4-MCP, (b) 4-MPBA, and (c) 4-MBA with Au NRs and NFs.

the aromatic ring breathing and C–S stretching modes caused by Au NFs were found to be 12.74 cm^{-1} and 3.02 cm^{-1}, respectively, for 4-MCP molecules with respect to the SERS peak position generated by Au NRs. Similarly, such peak shifts were found to be 2.88 cm^{-1} and 0.6 cm^{-1}, respectively, for 4-MPBA, and 2.53 cm^{-1} and 1.52 cm^{-1}, respectively, for 4-MBA molecules. The larger peak shifts in aromatic ring breathing vibration modes caused by Au NFs may be due to a possible strain effect instigated by their unique anisotropic geometry to a more parallel orientation.[51] The close proximity of the C–S bond to the Au NS surface, regardless of the structures, could be responsible for less or negligible changes in the SERS peak position for these molecules. Furthermore, the larger SERS peak position shift assigned to the aromatic ring breathing mode for 4-MCP molecules (12.74 cm^{-1}) may be due to an even lower density of this molecule bonded to Au NFs, so that the strain effect caused by Au NFs can be more dominant. This is possible due to the relatively less hydrophilic nature of 4-MCP molecules. The presence of benzene rings on all these molecules increases hydrophobicity. The presence of the boronic acid group and carboxyl group in 4-MPBA and 4-MBA molecules, respectively, can increase hydrophilicity, while the presence of only one hydroxyl group in 4-MCP is responsible for adding hydrophilicity.

Regardless of aromatic ring breathing and C–S stretching modes, we observed the emergence of numerous SERS peaks of these reporter molecules from a few local regions of Au NF arrays, while we did not see such a variation with Au NR arrays. Fig. 4 shows the comparison of such Au NF array assisted SERS signals of selected reporter molecules with respect to SERS signals assisted by Au NR arrays. The dramatic change in the SERS signals caused by Au NFs could be due to the collection of SERS signals from the region where the density of reporter molecules is relatively low. The availability of a few such local regions in the Au NF arrays is possible due to their anisotropic and relatively large lateral surface area. In such a case, a more parallel orientation of reporter molecules on the Au NF surface can still be expected due to minimal or no steric repulsion between adsorbed molecules. This, in turn, can enhance the SERS signals of various vibrational modes that come into proximity with the Au NFs. We also validated the concentration-dependent SERS activity of 4-MCP molecules with Au NSs in the range of 100 mM to 0.0001 mM (SI Fig. S2). We observed the emergence of multiple SERS peaks with Au NRs at very low concentrations, particularly below 0.01 mM, supporting the correlation of SERS sensitivity with molecular density, which is believed to control molecular orientations, while Au NFs support more parallel orientation despite the concentration changes due to their special hierarchical geometry. Upon comparing the Au NF assisted SERS signals of all these reporter molecules, we observed that SERS sensitivity is much stronger

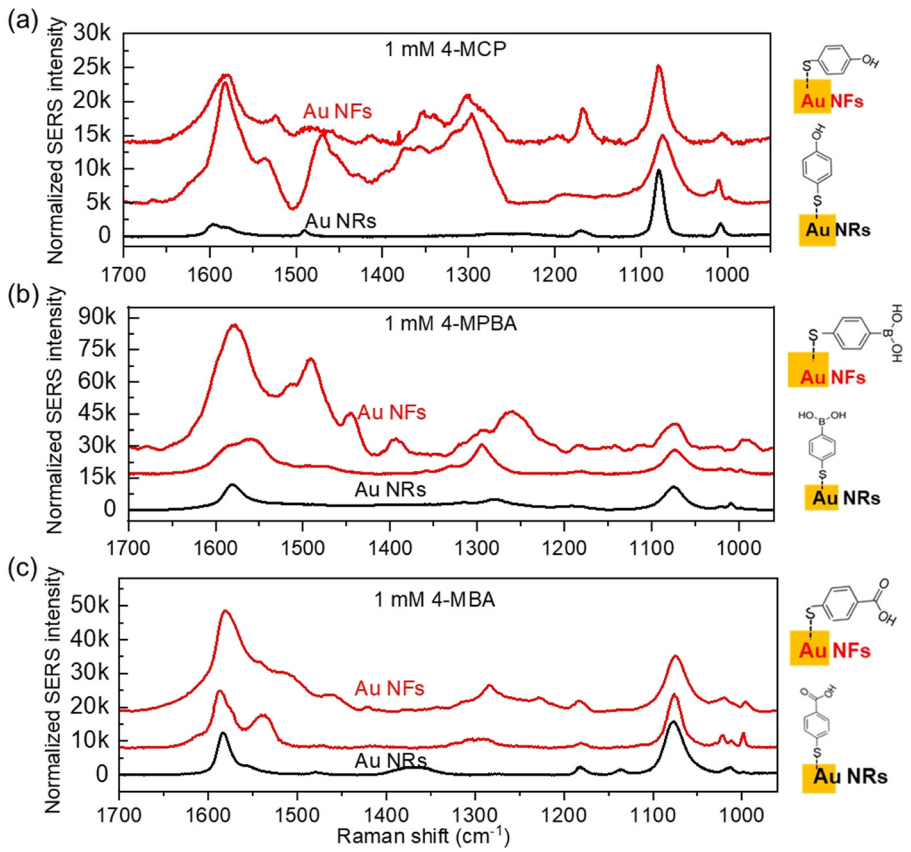

Fig. 4 Observation of several SERS peaks with Au NFs. Enhancement of relative SERS intensity of many bond vibrations of (a) 4-MCP, (b) 4-MPBA, and (c) 4-MBA molecules at their 1 mM concentration.

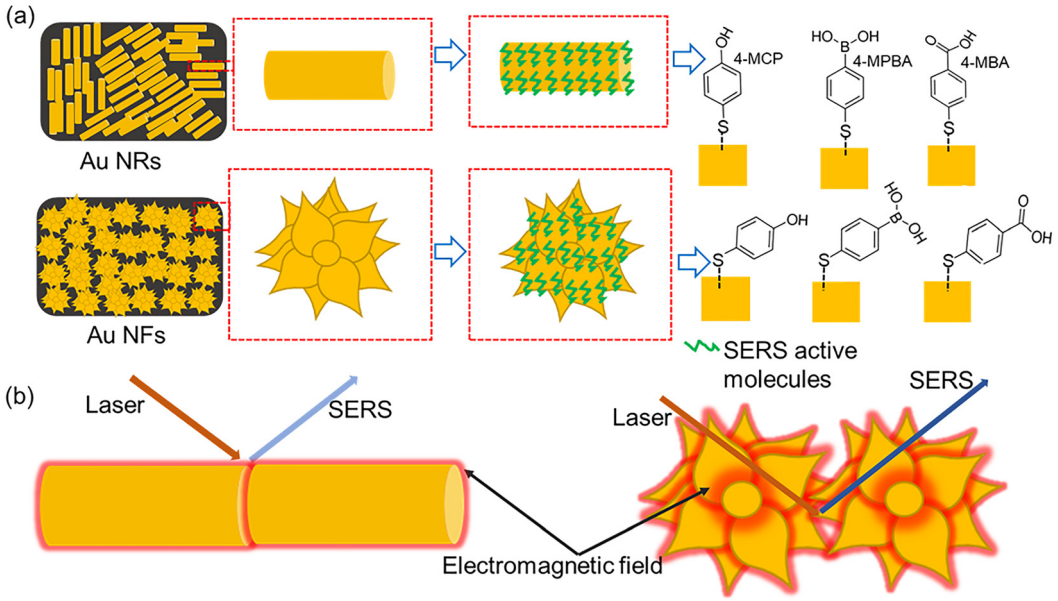

Fig. 5 Schematic illustrations of metallic nanostructures' functionalization and their SERS active sites. (a) Arrays of Au NRs and Au NFs, functionalization with different functional reporter molecules and expected molecular orientations. (b) Distribution of electromagnetic fields around Au NRs and NFs under laser excitation and generation of SERS signals.

with 4-MCP molecules, which could be due to the collection of signals from the region with even lower molecular density.

We conceptualized the phenomenon of Au NRs and Au NFs assisting SERS phenomena in Fig. 5. Fig. 5(a) shows schematic images of the decoration of Au NSs on Si chips, their bonding with reporter molecules, 4-MCP, 4-MPBA and 4-MBA, and possible molecular orientations with respect to the different geometries of Au NRs and NFs. Furthermore, Fig. 5(b) illustrates the schematic images showing the possible electromagnetic field strength of Au NR and NF arrays responsible for the generation of the SERS effect. Future theoretical and more controlled experimental studies, particularly monitoring the exact density of Au NFs and adsorbed reporter molecules, can provide a much deeper understanding of this phenomenon.

Specifically towards sensing applications, Au NF arrays functionalized with 4-MBA molecules can deliver highly efficient pH sensors as the carboxylate stretching mode of 4-MBA molecules in the range of 1400–1425 cm^{-1} has been reported to be highly pH-sensitive in earlier studies.[7,31] Moreover, Au NF arrays functionalized with these reporter molecules can also lead to the development of a highly efficient glucose sensor, as the OH molecules in these reporter molecules, 4-MCP, 4-MPBA and 4-MBA, can bind with glucose molecules. Earlier studies have reported that the aromatic ring breathing and C–S stretching Raman active modes at 1588 cm^{-1} and 1072 cm^{-1}, respectively, are highly glucose sensitive.[20,51] Studying the pH values and glucose concentration-dependent SERS activities assisted by Au NFs under the well-controlled density of Au NFs and functional molecules adsorbed to Au NF arrays will be the future scope of the study. Decorations of Au NFs to polymeric microneedles can provide the opportunity for *in vivo* pH and glucose sensing *via* punching on the skin to collect epidermal fluids for analysis. However, Au NF decorated polymeric microneedles first require *ex vivo* testing to evaluate SRRS performance, investigating the mechanical strength of microneedles, toxicity and the lifetime of the sensor in the skin and performance in animal models, all of which are the future direction of our study.

Conclusions

We reported the SERS activity of Au NRs and Au NFs for a few thiol derivative aromatic reporter molecules, 4-MBA, 4-MPBA and 4-MCP, respectively. We comprehensively monitored the interactions of Au NFs and Au NRs with reporter molecules. We demonstrated that Au NFs provide significantly enhanced relative SERS intensity of various possible bond vibrations of reporter molecules compared to Au NRs, which possibly arises from the suitable integration of hot spots and relatively parallel molecular orientation to Au NFs. Many of those bond vibrations of these selective reporter molecules have been used as biomarkers for pH and glucose sensing, which is very important in medical diagnosis of various diseases. Overall, this study presents a new strategy to increase SERS sensitivity, which can be applied for sensing a variety of relevant analytes in various bodily fluids. We believe that this study can be useful for advancing the understanding of SERS phenomena as well as designing a suitable bio/chemical sensor.

Experimental section

Chemicals and materials

Many chemicals including hydroxylamine hydrochloride ($NH_2OH{\cdot}HCl$) ($\geq$99.0%), tetrachloroauric(III) acid ($HAuCl_4{\cdot}3H_2O$, 99.9%), silver nitrate ($AgNO_3$, $\geq$99%), cetyltrimethylammonium

bromide (CTAB, ~98%), 4-mercaptophenol (4-MCP, 99%), polyvinylpyrrolidone (PVP), and silicon wafer were bought from Fisher Scientific. Similarly, sodium hydroxide (NaOH, >98%), sodium citrate, trisodium salt, dihydrate (≥99.0%), L-ascorbic acid (>99%), and citric acid anhydrous (>99.5%) were purchased from DOT Scientific. Sodium borohydride ($NaBH_4$, 99.9%), 4-mercaptobenzoic acid (4-MBA, 99%), 4-mercaptophenylboronic acid (4-MPBA, 90%), and hydrochloric acid (HCl, 37%) were obtained from Millipore Sigma. We used all the reagents directly without further purification.

Instrumentation

UV-vis light extinction measurements. A Beckman Coulter Du-800 spectrophotometer was used to collect UV-vis spectra of Au NS colloidal solutions.

Oxygen plasma etcher. A PELCO easiGlow™ system was used for the oxygen plasma treatment.

SERS measurements. A LabRAM HR Evolution Confocal Raman Microscope was used for SERS spectral measurements. A long working distance, 100× air objective lens with a numerical aperture of 0.85 was used to excite the sample and collect the SERS signals. A 785 nm wavelength continuous wave diode laser was chosen for the SERS measurements, and the laser spot size was ~1.1 micron. All SERS data were collected with a laser excitation power of ~2 mW and an exposure time of 10 seconds. The spectral resolution of this system is lower than 1 cm^{-1}.

SEM images. A JEOL JSM-7900FLV instrument was used to image Au NSs.

Conflicts of interest

The authors declare no competing interest.

Data availability

All data of this study are available within the paper and its supplementary information (SI).

Supplementary information is available. See DOI: https://doi.org/10.1039/d5tc02771c.

Acknowledgements

The authors acknowledge Professor Milan Mrksich and Dr Eric J. Berns for providing lab facility and constructive discussions during data analysis. This work made use of the EPIC, SPID, and NUFAB facilities of Northwestern University's NUANCE Center, which has received support from the SHyNE Resource (NSF ECCS-2025633), the IIN, and Northwestern's MRSEC program (NSF DMR-2308691 and NSF DMR-1720139).

References

1 J. Langer, D. Jimenez de Aberasturi, J. Aizpurua, R. A. Alvarez-Puebla, B. Auguié, J. J. Baumberg, G. C. Bazan, S. E. J. Bell, A. Boisen and A. G. Brolo, *et al.*, Present and Future of Surface-Enhanced Raman Scattering, *ACS Nano*, 2020, **14**(1), 28–117, DOI: 10.1021/acsnano.9b04224.

2 M. Moskovits and B. D. Piorek, A brief history of surface-enhanced Raman spectroscopy and the localized surface plasmon Dedicated to the memory of Richard Van Duyne (1945–2019), *J. Raman Spectrosc.*, 2021, **52**(2), 279–284, DOI: 10.1002/jrs.6028.

3 S. Shim, C. M. Stuart and R. A. Mathies, Resonance Raman Cross-Sections and Vibronic Analysis of Rhodamine 6G from Broadband Stimulated Raman Spectroscopy, *Chem. Phys. Chem.*, 2008, **9**(5), 697–699, DOI: 10.1002/cphc.200700856.

4 L. M. Almehmadi, S. M. Curley, N. A. Tokranova, S. A. Tenenbaum and I. K. Lednev, Surface Enhanced Raman Spectroscopy for Single Molecule Protein Detection, *Sci. Rep.*, 2019, **9**(1), 12356, DOI: 10.1038/s41598-019-48650-y.

5 S.-C. Luo, K. Sivashanmugan, J.-D. Liao, C.-K. Yao and H.-C. Peng, Nanofabricated SERS-active substrates for single-molecule to virus detection in vitro: A review, *Biosens. Bioelectron.*, 2014, **61**, 232–240, DOI: 10.1016/j.bios.2014.05.013.

6 B. Sharma, R. R. Frontiera, A.-I. Henry, E. Ringe and R. P. Van Duyne, SERS: Materials, applications, and the future, *Mater. Today*, 2012, **15**(1), 16–25, DOI: 10.1016/S1369-7021(12)70017-2.

7 J. E. Park, N. Yonet-Tanyeri, E. Vander Ende, A.-I. Henry, B. E. Perez White, M. Mrksich and R. P. Van Duyne, Plasmonic Microneedle Arrays for *in Situ* Sensing with Surface-Enhanced Raman Spectroscopy (SERS), *Nano Lett.*, 2019, **19**(10), 6862–6868, DOI: 10.1021/acs.nanolett.9b02070.

8 X. X. Han, R. S. Rodriguez, C. L. Haynes, Y. Ozaki and B. Zhao, Surface-enhanced Raman spectroscopy, *Nat. Rev. Methods Primers*, 2022, **1**(1), 87, DOI: 10.1038/s43586-021-00083-6.

9 X. Liang, N. Li, R. Zhang, P. Yin, C. Zhang, N. Yang, K. Liang and B. Kong, Carbon-based SERS biosensor: from substrate design to sensing and bioapplication, *NPG Asia Mater.*, 2021, **13**(1), 8, DOI: 10.1038/s41427-020-00278-5.

10 H. Chang, W. Hur, H. Kang and B.-H. Jun, *In vivo* surface-enhanced Raman scattering techniques: nanoprobes, instrumentation, and applications, *Light: Sci. Appl.*, 2025, **14**(1), 79, DOI: 10.1038/s41377-024-01718-5.

11 C. Lin, Y. Li, Y. Peng, S. Zhao, M. Xu, L. Zhang, Z. Huang, J. Shi and Y. Yang, Recent development of surface-enhanced Raman scattering for biosensing, *J. Nanobiotechnol.*, 2023, **21**(1), 149, DOI: 10.1186/s12951-023-01890-7.

12 G. C. Schatz, SERS and the scientific career of Richard P. Van Duyne (1945–2019), *J. Raman Spectrosc.*, 2021, **52**(2), 268–278, DOI: 10.1002/jrs.6052.

13 S. Lin, M. Dong, C. Li, X. Lin, Y. Cong, W. Xu, Z. Bao and B. Dong, Machine Learning-assisted Ultrasensitive SERS Immunoassays Across Wide Concentration Ranges Toward Clinical Ovarian Cancer Diagnosis, *Adv. Funct. Mater.*, 2025, e09813, DOI: 10.1002/adfm.202509813.

14 X. Wang, W. Hasi, S. Lin, S. Han, G. Fang and X. Lin, Plasmonic Nanocavities with Metallic Spacer Layers for

Ultrasensitive Detection of Cr6+ Ions, *ACS Photonics*, 2025, **12**(7), 3754–3762, DOI: **10.1021/acsphotonics.5c00721**.

15 G. Fang, X. Lin, J. Wu, W. Xu, W. Hasi and B. Dong, Porous Nanoframe Based Plasmonic Structure With High-Density Hotspots for the Quantitative Detection of Gaseous Benzaldehyde, *Small*, 2025, **21**(7), 2408670, DOI: **10.1002/smll.202408670**.

16 K. M. R. Scher, Z. Wang, A. Nair, Y. Wu, M. Bartoli, M. Rovere, A. Tagliaferro, S. Rangan, L. Wang and L. Fabris, Concentration and Surface Chemistry Dependent Analyte Orientation on Nanoparticle Surfaces, *J. Phys. Chem. C*, 2022, **126**(38), 16499–16513, DOI: **10.1021/acs.jpcc.2c05007**.

17 C. Sun, T. Chen, W. Ruan, B. Zhao and Q. Cong, Controlling the orientation of probe molecules on surface-enhanced Raman scattering substrates: A novel strategy to improve sensitivity, *Anal. Chim. Acta*, 2017, **994**, 65–72, DOI: **10.1016/j.aca.2017.10.004**.

18 C. Sun, T. Chen, W. Ruan, Y. M. Jung, Q. Cong and B. Zhao, A simple strategy to improve the sensitivity of probe molecules on SERS substrates, *Talanta*, 2019, **195**, 221–228, DOI: **10.1016/j.talanta.2018.11.040**.

19 S. Li, Q. Zhou, W. Chu, W. Zhao and J. Zheng, Surface-enhanced Raman scattering behaviour of 4-mercaptophenyl boronic acid on assembled silver nanoparticles, *Phys. Chem. Chem. Phys.*, 2015, **17**(27), 17638–17645, DOI: **10.1039/C5CP02409A**.

20 D. Yang, S. Afroosheh, J. O. Lee, H. Cho, S. Kumar, R. H. Siddique, V. Narasimhan, Y.-Z. Yoon, A. T. Zayak and H. Choo, Glucose Sensing Using Surface-Enhanced Raman-Mode Constraining, *Anal. Chem.*, 2018, **90**(24), 14269–14278, DOI: **10.1021/acs.analchem.8b03420**.

21 J. Chen, J. Wang, Y. Geng, J. Yue, W. Shi, C. Liang, W. Xu and S. Xu, Single-Cell Oxidative Stress Events Revealed by a Renewable SERS Nanotip, *ACS Sens.*, 2021, **6**(4), 1663–1670, DOI: **10.1021/acssensors.1c00395**.

22 V. Kumar Singh, V. Kumar Singh, A. Mishra, Varsha, A. Abha Singh, G. Prasad and A. Kumar Singh, Recent advancements in coordination compounds and their potential clinical application in the management of diseases: An up-to-date review, *Polyhedron*, 2023, **241**, 116485, DOI: **10.1016/j.poly.2023.116485**.

23 R. Monreal-Corona, X. Ribas, A. Pla-Quintana and A. Poater, Mechanism of Gold-Catalyzed Arylation-Lactonization: A Density Functional Theory Study on the Role of the (MIC^N)AuCl Complex in Au(I)/Au(III) Catalysis, *Inorg. Chem.*, 2025, **64**(25), 12755–12761, DOI: **10.1021/acs.inorgchem.5c01666**.

24 G. P. Neupane, M. D. Tran, S. J. Yun, H. Kim, C. Seo, J. Lee, G. H. Han, A. K. Sood and J. Kim, Simple Chemical Treatment to n-Dope Transition-Metal Dichalcogenides and Enhance the Optical and Electrical Characteristics, *ACS Appl. Mater. Interfaces*, 2017, **9**(13), 11950–11958, DOI: **10.1021/acsami.6b15239**.

25 G. P. Neupane, B. Wang, M. Tebyetekerwa, H. T. Nguyen, M. Taheri, B. Liu, M. Nauman and R. Basnet, Highly Enhanced Light–Matter Interaction in MXene Quantum Dots–Monolayer WS2 Heterostructure, *Small*, 2021, **17**(11), 2006309, DOI: **10.1002/smll.202006309**.

26 G. P. Neupane, K. P. Dhakal, E. Cho, B.-G. Kim, S. Lim, J. Lee, C. Seo, Y. B. Kim, M. S. Kim and J. Kim, *et al.*, Enhanced luminescence and photocurrent of organic microrod/ZnO nanoparticle hybrid system: Nanoscale optical and electrical characteristics, *Electron. Mater. Lett.*, 2015, **11**(5), 741–748, DOI: **10.1007/s13391-015-4496-0**.

27 M.-j Jin, J. Jo, G. P. Neupane, J. Kim, K.-S. An and J.-W. Yoo, Tuning of undoped ZnO thin film *via* plasma enhanced atomic layer deposition and its application for an inverted polymer solar cell, *AIP Adv.*, 2013, **3**(10), 102114, DOI: **10.1063/1.4825230**(acccessed 2/14/2025).

28 G. P. Neupane, W. Ma, T. Yildirim, Y. Tang, L. Zhang and Y. Lu, 2D organic semiconductors, the future of green nanotechnology, *Nano Mater. Sci.*, 2019, **1**(4), 246–259, DOI: **10.1016/j.nanoms.2019.10.002**.

29 G. P. Neupane, M. D. Tran, H. Kim and J. Kim, Modulation of Optical and Electrical Characteristics by Laterally Stretching DNAs on CVD-Grown Monolayers of MoS2, *J. Nanomater.*, 2017, **2017**(1), 2565703, DOI: **10.1155/2017/2565703**.

30 G. P. Neupane, Introduction, in *Anisotropic 2D Materials and Devices*, ed. Lu, Y., *The Royal Society of Chemistry*, 2022.

31 M. Pacaud, K. Hervé-Aubert, M. Soucé, A. A. Makki, F. Bonnier, A. Fahmi, A. Feofanov and I. Chourpa, One-step synthesis of gold nanoflowers of tunable size and absorption wavelength in the red & deep red range for SERS spectroscopy, *Spectrochim. Acta, Part A*, 2020, **225**, 117502, DOI: **10.1016/j.saa.2019.117502**.

32 I. S. Tódor, L. Szabó, O. T. Marişca, V. Chiş and N. Leopold, Gold nanoparticle assemblies of controllable size obtained by hydroxylamine reduction at room temperature, *J. Nanopart. Res.*, 2014, **16**(12), 2740, DOI: **10.1007/s11051-014-2740-4**.

33 D. Goia and E. Matijević, Tailoring the particle size of monodispersed colloidal gold, *Colloids Surf., A*, 1999, **146**(1), 139–152, DOI: **10.1016/S0927-7757(98)00790-0**.

34 T. K. Sau and C. J. Murphy, Seeded High Yield Synthesis of Short Au Nanorods in Aqueous Solution, *Langmuir*, 2004, **20**(15), 6414–6420, DOI: **10.1021/la049463z**.

35 R. E. Darienzo, O. Chen, M. Sullivan, T. Mironava and R. Tannenbaum, Au nanoparticles for SERS: Temperature-controlled nanoparticle morphologies and their Raman enhancing properties, *Mater. Chem. Phys.*, 2020, **240**, 122143, DOI: **10.1016/j.matchemphys.2019.122143**.

36 P. Aldeanueva-Potel, E. Carbó-Argibay, N. Pazos-Pérez, S. Barbosa, I. Pastoriza-Santos, R. A. Alvarez-Puebla and L. M. Liz-Marzán, Spiked Gold Beads as Substrates for Single-Particle SERS, *Chem. Phys. Chem.*, 2012, **13**(10), 2561–2565, DOI: **10.1002/cphc.201101014**.

37 D.-A. Roşca, J. A. Wright and M. Bochmann, An element through the looking glass: exploring the Au–C, Au–H and Au–O energy landscape, *Dalton Trans.*, 2015, **44**(48), 20785–20807, DOI: **10.1039/C5DT03930D**.

38 T. Suni, K. Henttinen, I. Suni and J. Mäkinen, Effects of Plasma Activation on Hydrophilic Bonding of Si and SiO_2,

J. Electrochem. Soc., 2002, **149**(6), G348, DOI: **10.1149/1.1477209**.

39 R. Sánchez-González, E. Imbarack, C. Suazo, J. P. Soto, P. Leyton, S. Sánchez-Cortés and M. Campos-Vallette, Synthesis, characterization and surface enhanced Raman spectroscopy study of a new family of different substituted cruciform molecular systems deposited on gold nanoparticles, *J. Raman Spectrosc.*, 2021, **52**(5), 959–970, DOI: **10.1002/jrs.6082**.

40 K. T. Carron and L. G. Hurley, Axial and azimuthal angle determination with surface-enhanced Raman spectroscopy: thiophenol on copper, silver, and gold metal surfaces, *J. Phys. Chem.*, 1991, **95**(24), 9979–9984, DOI: **10.1021/j100177a068**.

41 S. Kaneko, D. Murai, S. Marqués-González, H. Nakamura, Y. Komoto, S. Fujii, T. Nishino, K. Ikeda, K. Tsukagoshi and M. Kiguchi, Site-Selection in Single-Molecule Junction for Highly Reproducible Molecular Electronics, *J. Am. Chem. Soc.*, 2016, **138**(4), 1294–1300, DOI: **10.1021/jacs.5b11559**.

42 H.-T. Rong, S. Frey, Y.-J. Yang, M. Zharnikov, M. Buck, M. Wühn, C. Wöll and G. Helmchen, On the Importance of the Headgroup Substrate Bond in Thiol Monolayers: A Study of Biphenyl-Based Thiols on Gold and Silver, *Langmuir*, 2001, **17**(5), 1582–1593, DOI: **10.1021/la0014050**.

43 M. A. Bryant and J. E. Pemberton, Surface Raman scattering of self-assembled monolayers formed from 1-alkanethiols: behavior of films at gold and comparison to films at silver, *J. Am. Chem. Soc.*, 1991, **113**(22), 8284–8293, DOI: **10.1021/ja00022a014**.

44 G. E. Poirier and E. D. Pylant, The Self-Assembly Mechanism of Alkanethiols on Au(111), *Science*, 1996, **272**(5265), 1145–1148, DOI: **10.1126/science.272.5265.1145**.

45 P. E. Scopelliti, A. Borgonovo, M. Indrieri, L. Giorgetti, G. Bongiorno, R. Carbone, A. Podestà and P. Milani, The Effect of Surface Nanometre-Scale Morphology on Protein Adsorption, *PLoS One*, 2010, **5**(7), e11862, DOI: **10.1371/journal.pone.0011862**.

46 X. Wang, X. Du, W. Guang, J. Zhou, G. Wang, D. Zhang, N. Abbas, Y. Jia, Y. Cheng and H. Wang, *et al.*, Effect of three-dimensional surface roughness on CH4 adsorption and diffusion in coal nanopores, *Phys. Fluids*, 2024, **36**(11), 112033, DOI: **10.1063/5.0238668** (acccessed 10/21/2025).

47 Y. Yang, S. Knust, S. Schwiderek, Q. Qin, Q. Yun, G. Grundmeier and A. Keller, Protein Adsorption at Nanorough Titanium Oxide Surfaces: The Importance of Surface Statistical Parameters beyond Surface Roughness, *Nanomaterials*, 2021, **11**(2), 357.

48 R. Hou, C. Zhang, L. Xu, Y. Ding and W. Xu, Construction of metal–organic nanostructures and their structural transformations on metal surfaces, *Phys. Chem. Chem. Phys.*, 2025, **27**(17), 8635–8655, DOI: **10.1039/D5CP00030K**.

49 E. Villarreal, G. G. Li, Q. Zhang, X. Fu and H. Wang, Nanoscale Surface Curvature Effects on Ligand–Nanoparticle Interactions: A Plasmon-Enhanced Spectroscopic Study of Thiolated Ligand Adsorption, Desorption, and Exchange on Gold Nanoparticles, *Nano Lett.*, 2017, **17**(7), 4443–4452, DOI: **10.1021/acs.nanolett.7b01593**.

50 K. Randazzo, M. Bartkiewicz, B. Graczykowski, D. Cangialosi, G. Fytas, B. Zuo and R. D. Priestley, Direct Visualization and Characterization of Interfacially Adsorbed Polymer atop Nanoparticles and within Nanocomposites, *Macromolecules*, 2021, **54**(21), 10224–10234, DOI: **10.1021/acs.macromol.1c01557**.

51 S. J. Lee, H. Jang and D. N. Lee, Recent advances in nanoflowers: compositional and structural diversification for potential applications, *Nanoscale Adv.*, 2023, **5**(19), 5165–5213, DOI: **10.1039/D3NA00163F**.

